

Robust fault detection, isolation and accommodation of current sensors in grid side converters

Panayiotis M. Papadopoulos, *Student Member, IEEE*, Lenos Hadjidemetriou, *Member, IEEE*,
Elias Kyriakides, *Senior Member, IEEE* and Marios M. Polycarpou, *Fellow, IEEE*

Abstract—The integration of modern renewable energy sources is enabled by the Grid Side Converter (GSC) based on power electronic technology. The operation of the GSC is properly regulated by the GSC controller according to sensor measurements (i.e., of the grid voltage, of the line currents, and of the voltage at the DC-link). However, in case of current sensor faults, the operation of the GSC and of the entire renewable system can be critically affected and catastrophic failures may occur if the sensor fault is not accommodated on time. This paper proposes a model-based Fault Detection, Isolation and Accommodation (FDIA) scheme, which enables the GSC to overcome faults that may occur on the associated current sensors. The sensor fault detection and isolation scheme has been designed based on analytical redundancy relations, while the accommodation of the faults is based on an adaptive estimation scheme. The proposed FDIA scheme has been applied on a modern GSC and the effectiveness of the scheme has been tested under several multiple current sensor faults and under several grid conditions. Furthermore, the FDIA scheme enables the GSC to operate properly (without causing failures or damages to its components) under current sensor faults and thus, the reliability of the GSC is enhanced.

Index Terms—Fault accommodation, fault detection, fault isolation, grid side converter, sensor faults.

I. INTRODUCTION

THE key technology for interconnecting Renewable Energy Sources (RES) is the power electronics based Grid Side Converter (GSC) [1]. The high penetration of RES [2] can downgrade the power quality and stability of the power system, as demonstrated in [3]–[6]. Thus, the recently issued international standards and local grid regulations [4], [6] require that the modern RES should ensure a proper operation of the power system under any condition. Accordingly, advanced GSC controllers are responsible for enabling a high quality current injection under any harmonic distorted condition and for providing an appropriate support to the electrical network under grid faults (i.e., short-circuit events in the power grid). One of the most essential parts of the a three phase GSC is the associate controller (see Fig. 1). The GSC controller operates based on: (i) three voltage sensors for measuring

This work was partially supported by the European Research Council (ERC) under the ERC Advanced Grant FAULT-ADAPTIVE, and the Research Promotion Foundation (RPF, Cyprus, Project KOINA/SOLAR-ERA.NET/0114/02), by Energinet.dk (ForskEL, Denmark) and the SOLAR-ERA.NET (European Unions Seventh Framework Programme).

Panayiotis M. Papadopoulos, Lenos Hadjidemetriou, Elias Kyriakides and Marios M. Polycarpou are with KIOS Research Center for Intelligent Systems and Networks, Department of Electrical and Computer Engineering, University of Cyprus, Nicosia, 1678, Cyprus (email:papadopoulos.panayiotis@ucy.ac.cy, hadjidemetriou.lenos@ucy.ac.cy, elias@ucy.ac.cy, mpolycar@ucy.ac.cy)

the grid voltage and three current sensors for measuring the injected currents, (ii) an advanced synchronization method, (iii) an active and reactive power controller (*PQ* controller), and (iv) a robust current controller against harmonics as shown in [7]. Since the operation of the GSC controller relies on the sensor measurements, it is unavoidable that the GSC response can be affected by sensor failures. Thus, a sensor fault can lead to a catastrophic failure of the GSC and consequently the overall RES will be affected. Such failures cause high maintenance costs for replacing the affected components or even the entire GSC (i.e, increasing capital outlays) and loss of energy/income produced by RES. The prevention of the aforementioned effects leads to the development and application of sensor Fault Detection Isolation and Accommodation (FDIA) techniques.

Most of the literature on fault diagnosis in power electronics converters focuses on actuator faults [8], [9]. Specifically, in [8], a model-based fault detection and localization method is proposed considering only open-circuit semiconductor failures while in [9], an artificial neural network method is proposed for detecting and localizing short- and open- circuit actuator faults. Several works of the same group, [10]–[12], deployed model-free methodologies in order to diagnose open-circuited faults in inverters and unbalanced faults in rectifiers. All the above-mentioned works consider healthy sensors.

However, sensor failures are highly possible and can damage the converters. Despite that, limited attention was so far given on sensor faults. Two model-based current sensor fault detection schemes for doubly-fed induction generators are proposed in [13], [14], based on parity equations and on observers, re-

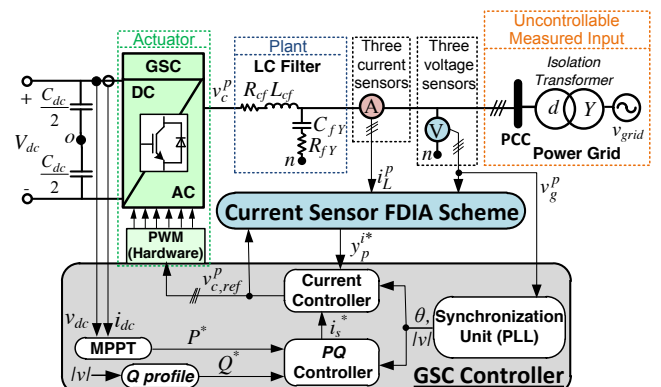


Fig. 1. Structure of an interconnected GSC along with its controller and the proposed current sensor FDIA scheme.

spectively. Recently, it has been proposed a model-based fault diagnosis approach. This approach can be applied to several types of faults, including sensor faults (i.e., voltage and current sensor faults) on the DC-side of a PV application [15]. This approach focuses only on the DC-DC boost converter. It is worth mentioning that the accommodation of sensor faults is not addressed in [13]–[15]. A sensor fault accommodation method for GSC, is presented in [16] in which the detection is based on a prediction algorithm. In this case the accommodation of a sensor fault relies on the physical redundancy of a three-wire interconnection (using $\sum_{p \in \{a,b,c\}} i_L^p = 0$ of Kirchhoff's Current Law) and unfortunately this method cannot consider multiple sensor faults. Further, such accommodation technique can not directly be applied on a single phase GSCs (i.e., for residential RES), since the physical redundancy does not exist in these systems. In the previous-mentioned works, the performance of the fault diagnosis schemes is not examined under grid short-circuit events, highly harmonic distortion conditions, and abrupt changes in operating power set-points which may affect the robustness of a fault diagnosis methodology.

The contribution of this paper is the development of a model-based FDIA methodology on the controller of a three-phase GSC, which in real-time, can detect, isolate, and accommodate single and multiple current sensor faults. The proposed current sensor fault detection method relies on analytical redundancy relations based on residuals and adaptive thresholds. Residuals describe discrepancies between the process and the model, while thresholds are bounds on the residuals, designed for the fault-free case, taking into account modeling uncertainties and unknown disturbances [17], [18]. In addition, the proposed detection and isolation scheme has been enhanced in a way to achieve a proper operation under any possible operating scenarios for the GSC (i.e., balanced and unbalanced grid faults, highly harmonic distortion conditions, and abrupt variations of the power injection). Further, an accommodation methodology has been developed according to adaptive estimation scheme, which enables the proper operation of the GSC even under multiple sensor faults. It is notable that under single sensor faults, for the accommodation method there is an opportunity of choosing between the adaptive estimation scheme and the physical redundancy is constrained on the three-wire interconnection of the GSC. The proposed FDIA has been developed and applied on a modern GSC for interconnecting RES, which can operate properly under any grid condition, as required by the grid regulations. The simulation and experimental results demonstrate that the developed FDIA scheme can properly detect, isolate and accommodate faults on any current sensors. The proposed FDIA scheme ensures a proper operation of the GSC under sensor faults, which can increase the reliability of the GSC and can extend the lifetime of the entire RES.

This paper is organized as follows. In Section II, the problem is formulated, where the dynamic equations of the GSC and sensor fault configuration are presented in discrete time. In Section III the proposed FDIA scheme is designed. Finally, the developed FDIA scheme is validated with simulation and experimental results in Section IV, while the paper concludes in Section V.

II. PROBLEM FORMULATION

The aim of this paper is to propose a current sensor FDIA scheme that can be applied on a real-time GSC, which is responsible for the interconnection of RES. The FDIA scheme enables the proper operation of the GSC under current sensor faults by avoiding undesired failures that can cause serious damages to the GSC. Since the FDIA scheme is model-based, it is necessary to describe the entire system according to the corresponding electrical dynamic equations in discrete time.

According to Fig. 1, an interconnected GSC system consists of: (i) the GSC which is the actuator, (ii) the LC filter which is the plant, (iii) the power grid which can be considered as an uncontrollable measured input to the system, (iv) three voltage sensors for measuring the grid voltages v_g^p of each phase p at the Point of Common Coupling (PCC), (v) three current sensors for measuring the line current i_L^p of each phase p , and (vi) the GSC controller for regulating the overall operation of the system. The closed-loop GSC controller is responsible for generating the corresponding $v_{c,ref}^p$, that will be fed into the GSC through a hardware Pulse Width Modulation (PWM) in order to regulate the output voltage of the converter v_c^p .

The first-order linear discrete differential equation that determines the injected line currents of each phase $i_L^p(k+1)$ is given by,

$$i_L^p(k+1) = A i_L^p(k) + B \Delta V^p(k), \quad (1)$$

where k is the discrete time step, $p \in \mathcal{P} = \{a, b, c\}$ where the set \mathcal{P} depicts the phases of the three-phase system, and $\Delta V^p(k)$ is defined by the difference between the converter voltage ($v_c^p(k)$) and the grid voltage ($v_g^p(k)$) as,

$$\Delta V^p(k) = v_c^p(k) - v_g^p(k). \quad (2)$$

v_c^p is the p -phase converter voltage with the neutral-point (n) (see Fig. 1) as a reference and is given as,

$$v_c^p(k) = v_{co}^p(k) + v_{on}(k), \quad (3)$$

where v_{co}^p is the p -phase voltage of the converter with the DC-link mid-point (o) as a reference, which can be directly regulated by the controller output $v_{c,ref}^p(k)$ as shown in (4), and v_{on} is the voltage difference between the DC-link mid-point (o) and the neutral-point (n) as given in (5), where both are defined as follows:

$$v_{co}^p(k+1) = G v_{co}^p(k) + H v_{c,ref}^p(k), \quad (4)$$

$$v_{on}(k) = \frac{1}{3} \sum_{p \in \mathcal{P}} v_g^p(k). \quad (5)$$

The plant parameters A and B of (1) are defined according to the resistance (R_{cf}) and inductance (L_{cf}) parameters of the LC filter, the location of voltage and current sensors, and the sampling period T_s of the controller as follows,

$$A = \frac{L_{cf} - R_{cf} T_s}{L_{cf}}, \quad B = \frac{T_s}{L_{cf}}. \quad (6)$$

Further, for the actuator parameters G and H consider that the

response of the actuator presents 1.5 samples delay, such as,

$$G = \frac{1}{3}, \quad H = \frac{2}{3}. \quad (7)$$

For designing the model-based FDIA scheme, it is convenient to convert the dynamic equations of the system (1)-(7) in the following discrete-time state space form:

$$x_p(k+1) = (A + \Delta A) x_p(k) + (B + \Delta B) v_p(k) \quad (8)$$

$$- (B + \Delta B) d_p(k) + h_p(x_p(k)),$$

$$v_p(k+1) = G v_p(k) + H u_p(k), \quad (9)$$

where $x_p \doteq i_L^p$ is the state, $u_p \doteq v_{c,ref}^p$ is the GSC controller output, $v_p \doteq v_c^p$ is the GSC converter output (control input to the plant), and $d_p \doteq v_g^p$ is the uncontrollable (measured) input to the plant, which constitutes the grid voltage as represented in Fig. 2. ΔA , ΔB represent the parametric uncertainty due to manufacturing tolerance of the filter parameters (i.e., resistance, inductance) and $h_p(x_p)$ depicts the modeling uncertainty due to the current and voltage high-order harmonics and discretization error. Current and voltage sensors are installed in the GSC structure in order to provide sensing information to the GSC controller as it is presented in Fig. 1 and Fig. 2. The current and voltage sensors are configured as,

$$y_p^i(k) = x_p(k) + n_p^i(k) + \beta(k - K_p^f) f_p^i(k), \quad (10)$$

$$y_p^d(k) = d_p(k) + n_p^d(k), \quad (11)$$

where y_p^i is the current GSC measurements, y_p^d is the grid voltage measurements, n_p^i and n_p^d represent the noise corrupting the measurements of x_p and d_p , respectively, and $\beta(k - K_p^f) f_p^i(k)$ is the additive fault affecting the sensor measurements of the current at the GSC. The term f_p^i represents the fault magnitude and $\beta(k - K_p^f)$ is the time profile of the sensor fault such as,

$$\beta(k - K_p^f) = 1 - \exp(-\rho_p(k - K_p^f)), \quad (12)$$

where K_p^f is the time of fault occurrence and ρ_p is the evolution rate of the fault, which for abrupt sensor faults $\rho_p \rightarrow \infty$ [19].

III. METHODOLOGY

This section presents the main design guidelines of the proposed FDIA scheme for the GSC. The methodology relies on a model-based adaptive state estimation scheme. The detection of currents sensor faults is achieved by the development of analytical redundancy relations (ARRs), one for each phase. Each ARR is constructed by the output residual and the adaptive threshold. The violation of ARR detects the current sensor fault occurrence. Based on the ARR, an isolation decision logic is introduced in order to determine which phase is affected and also is responsible to distinguish between sensor faults and grid faults. After the isolation of a current fault, an adaptive estimation scheme is activated for sensor fault estimation. Thus, the estimation of the sensor fault is employed in the accommodation scheme, aiming to compensate the effects of faults in current sensors. It is noted that the proposed FDIA scheme has been designed to consider only additive sensor faults.

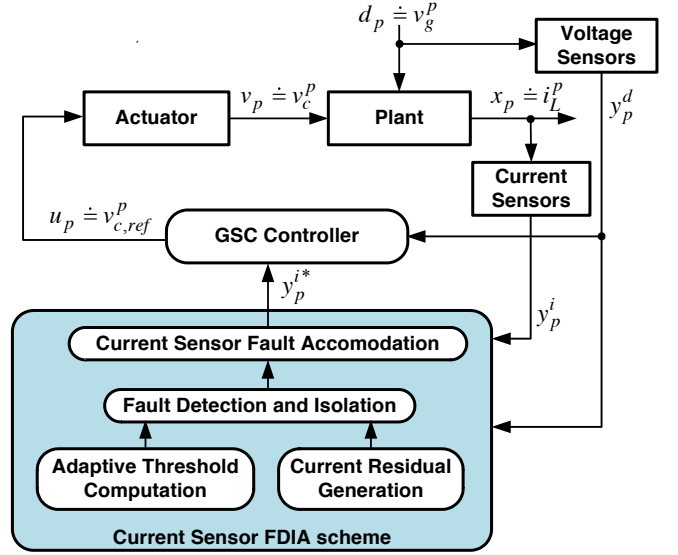


Fig. 2. Schematic representation of the entire system (i.e., actuator, plant, sensors, GSC controller and current sensor FDIA scheme).

A. Current residual generation

In order to detect the presence of current sensor faults, current residuals are constructed based on the knowledge of the system (i.e., sensor measurements) and the model (i.e., estimation of inverter's line currents). The estimation of the line currents is obtained by the following linear adaptive state estimation scheme of the p phase, $\forall p \in \mathcal{P}$ which is presented as follows,

$$\begin{aligned} \hat{x}_p(k+1) = & A \hat{x}_p(k) + B v_p(k) - B y_p^d(k) \\ & + \lambda_p^i (y_p^i(k) - \hat{x}_p(k) - \hat{f}_p^i(k)) \\ & + \Omega_p(k) (\hat{f}_p^i(k+1) - \hat{f}_p^i(k)), \end{aligned} \quad (13)$$

$$\Omega_p(k+1) = (A - \lambda_p^i) \Omega_p(k) - \lambda_p^i, \quad (14)$$

$$\hat{f}_p^i(k+1) - \hat{f}_p^i(k) = \frac{\gamma_p (\Omega_p(k) + 1)}{1 + \xi (\Omega_p(k) + 1)^2} \mathcal{D}_p [\varepsilon_{y_p}^i(k)], \quad (15)$$

with $x_p(0) = 0$ and $\Omega_p(k_D) = 0$ where k_D denotes the time step in which a sensor fault is detected and isolated. Further, \hat{x}_p is the estimation of the state x_p , λ_p^i is the observer gain and it is selected according to $|A - \lambda_p^i| \leq 1$ in order to satisfy the stability criterion for discrete-time dynamic systems [20], Ω_p is a filtering term [21] to ensure the stability property of the adaptive estimation scheme (see Appendix A), \hat{f}_p^i is the estimation of the sensor fault f_p^i which is activated when a fault is detected at k_D (with $\hat{f}_p^i(k_D) = 0$), γ_p is the learning rate of the adaptive law denoted in (15) and ξ is a design constant of the normalized gradient algorithm [22]. The output residual $\varepsilon_{y_p}^i$, $\forall p \in \mathcal{P}$ is defined as

$$\varepsilon_{y_p}^i(k) = y_p^i(k) - \hat{x}_p(k) - \hat{f}_p^i(k). \quad (16)$$

Hence, the state estimation error denoted by ε_{x_p} is defined as

$$\varepsilon_{x_p}^i(k) = x_p(k) - \hat{x}_p(k). \quad (17)$$

Note that, the dead zone operator denoted by $\mathcal{D}_p[\cdot]$ and used in (15) is defined in (24) in Section III-C.

B. Computation of adaptive threshold

Assumption 1: The parametric uncertainties ΔA , ΔB and modeling uncertainty $h_p(x_p)$ are uniformly bounded $\forall k$ such as $|\Delta A| \leq \overline{\Delta A}$, $|\Delta B| \leq \overline{\Delta B}$, $|h_p(x_p(k))| \leq \overline{h}_p$, for all $p \in \mathcal{P}$, where $\overline{\Delta A}$, $\overline{\Delta B}$ and \overline{h}_p are known constant bounds.

Assumption 2: The noise $n_p^i(k)$, $n_p^d(k)$ corrupting sensor measurements of y_p^i , y_p^d , are uniformly bounded $\forall k$ such as $|n_p^i(k)| \leq \overline{n}_p^i$ and $|n_p^d(k)| \leq \overline{n}_p^d$, for all $p \in \mathcal{P}$, where \overline{n}_p^i and \overline{n}_p^d are known constant bounds.

Note that the constant bounds $\overline{\Delta A}$, $\overline{\Delta B}$ and \overline{n}_p^i , \overline{n}_p^d are selected based on the manufacturing tolerances of the LC filter and current and voltage sensors, respectively. The constant bound \overline{h}_p represents the maximum bound on the effect of discretization error and high-order voltage and current harmonics. The values of all the above design parameters are given analytically in Table I.

The analytical redundancy relation (ARR) \mathcal{E}_p , for each $p \in \mathcal{P}$, is constructed under healthy conditions (i.e., $f_p^i = 0$) as follows,

$$\mathcal{E}_p : |\varepsilon_{y_p}^i(k)| \leq \overline{\varepsilon}_{y_p}^i(k), \quad (18)$$

where $\overline{\varepsilon}_{y_p}^i$ is the adaptive threshold and $\varepsilon_{y_p}^i$ can be analytically obtained by using (16) such as

$$\begin{aligned} \varepsilon_{y_p}^i(k+1) &= (A - \lambda_p^i) \varepsilon_{x_p}^i(k) + \Delta A x_p(k) \\ &\quad + \Delta B (v_p(k) - d_p(k)) + B n_p^d \\ &\quad + h_p(x_p(k)) - \lambda_p^i n_p^i(k) + n_p^i(k). \end{aligned} \quad (19)$$

It is worth mentioning that the solution of (19) can be numerically obtained as follows:

$$\begin{aligned} \varepsilon_{y_p}^i(k) &= (A - \lambda_p^i)^k \varepsilon_{x_p}^i(0) + \sum_{j=0}^{k-1} (A - \lambda_p^i)^{k-1-j} (\Delta A x_p(j) \\ &\quad + \Delta B (v_p(j) - d_p(j)) + B n_p^d(j) \\ &\quad + h_p(x_p(j)) - \lambda_p^i n_p^i(j) + n_p^i(k)). \end{aligned} \quad (20)$$

Hence, by applying the inequality of (18) on the residual of (20) and after some mathematical manipulations the adaptive threshold $\overline{\varepsilon}_{y_p}^i$, $\forall p \in \mathcal{P}$ is obtained as

$$\begin{aligned} \overline{\varepsilon}_{y_p}^i &= \alpha_p^k \overline{x}_p + \sum_{j=0}^{k-1} \alpha_p^{k-1-j} \overline{\Delta A} |\hat{x}_p(j)| + \sum_{j=0}^{k-1} \alpha_p^{k-1-j} \overline{\Delta A} \overline{\varepsilon}_{x_p}^i(j) \\ &\quad + \sum_{j=0}^{k-1} \alpha_p^{k-1-j} \overline{\Delta B} (|v_p(j) - y_p^d(j)| + \overline{n}_p^d) \\ &\quad + \sum_{j=0}^{k-1} \alpha_p^{k-1-j} (|\lambda_p^j| \overline{n}_p^i + \overline{h}_p) + \sum_{j=0}^{k-1} \alpha_p^{k-1-j} B \overline{n}_p^d + \overline{n}_p^i, \end{aligned} \quad (21)$$

where $|A - \lambda_p^i| \leq \alpha_p \leq 1$ and $|d_p(k)| \leq |y_p^d(k)| + \overline{n}_p^d$ since the sensor measurements of (11) are not affected by faults. Further, the $\overline{\varepsilon}_{x_p}^i$ is obtained as

$$\overline{\varepsilon}_{x_p}^i(k) = \varepsilon_1(k) + \sum_{j=0}^{k-1} \alpha_p^{k-1-j} \overline{\Delta A} \overline{\varepsilon}_{x_p}^i(j) \quad (22)$$

where

$$\begin{aligned} \varepsilon_1(k) &= \alpha_p^k \overline{x}_p + \sum_{j=0}^{k-1} \alpha_p^{k-1-j} \overline{\Delta A} |\hat{x}_p(j)| \\ &\quad + \sum_{j=0}^{k-1} \alpha_p^{k-1-j} \overline{\Delta B} (|v_p(j) - y_p^d(j)| + \overline{n}_p^d) \\ &\quad + \sum_{j=0}^{k-1} \alpha_p^{k-1-j} |\lambda_p^j| \overline{n}_p^i + \sum_{j=0}^{k-1} \alpha_p^{k-1-j} B \overline{n}_p^d. \end{aligned} \quad (23)$$

C. Current sensor fault detection and isolation logic

The detection is adequate to directly isolate the sensor faults (i.e., determine in which phase the fault occurred), since the \mathcal{E}_p ARR developed in (18) can be only affected by the sensor measurement y_p^i of the corresponding phase. Since y_p^d appears in the adaptive threshold of (21), it is important to note that the isolation logic assumes that the voltage sensor measurements of (11) will be healthy in order to avoid any false alarms.

In general a sensor fault is detected when the residual violates the corresponding adaptive threshold (i.e., $|\varepsilon_{y_p}^i(k)| > \overline{\varepsilon}_{y_p}^i(k)$). However, when an abrupt grid fault occurs (i.e., short circuit event in the power grid) it is highly possible that the proposed FDIA scheme will be affected resulting in a false sensor fault alarm. Therefore, there is a need to distinguish between a grid fault and a sensor fault. In order to distinguish the grid faults, the FDIA scheme is enhanced with a Grid Fault Classification Unit (GFCU), as has been proposed in [23]. The GFCU uses the synchronization signals that are estimated in real-time by an advanced phase-locked loop based synchronization method in order to detect a grid fault and further, to classify the fault in seven different categories (i.e., Type A-G as determined in [24]). The response time of the GFCU is less than 5 ms and thus it can be considered for the real-time grid fault detection. Therefore, a boolean decision signal G_f is constructed according to the GFCU output such that $G_f = 0$ under normal grid operation conditions and $G_f = 1$ when a grid fault occurs. As a conclusion, for each time step k the Algorithm 1 is executed in order to isolate the sensor faults (i.e., distinguish between sensor faults and grid faults). Note that the isolation decision signal D_p is also initialized in 0, such that $D_p(0) \leftarrow 0$.

Algorithm 1 Isolation Decision Logic of phase p

- 1: **if** ($|\varepsilon_{y_p}^i(k)| > \overline{\varepsilon}_{y_p}^i(k)$ **AND** $G_f(k) == 0$) **OR** $\Delta k_p > \overline{\Delta k}_p$
 - 2: $D_p \leftarrow 1$
 - 3: **elseif** ($|\varepsilon_{y_p}^i(k)| \leq \overline{\varepsilon}_{y_p}^i(k)$ **OR** $\Delta k_p \leq \overline{\Delta k}_p$) **AND** $G_f(k) == 1$
 - 4: $D_p \leftarrow 0$
-

In Algorithm 1, Δk_p is defined as $\Delta k_p = k - k_D$, where k_D denotes the time step in which the isolation decision signal $D_p(k_D)$ is set to 1 for the last time. The isolation decision signal D_p is set to one (i.e., $D_p \leftarrow 1$), when the ARR in (18) is violated and there is no grid fault according to GFCU (i.e., $G_f == 0$). The isolation decision signal D_p can only be reset to zero (i.e., $D_p \leftarrow 0$), when a grid fault is detected (i.e., $G_f == 1$) by the GFCU and the ARR in (18) are violated simultaneously or within a time less than the response time of the GFCU (i.e., 5 ms that corresponds to $\overline{\Delta k}_p$ samples).

A dead-zone operator \mathcal{D}_p is implemented in order to activate the adaptive law in (15) and it is defined as,

$$\mathcal{D}_p [\varepsilon_{y_p}^i(k)] = \begin{cases} \varepsilon_{y_p}^i(k), & D_p = 1 \\ 0, & D_p = 0 \end{cases}. \quad (24)$$

D. Current sensor fault accommodation

In the presence of additive sensor faults the following virtual sensor scheme is introduced to accommodate them. Each virtual sensor signal y_p^{i*} , $\forall p \in \mathcal{P}$ will be fed to the GSC controller in order to compensate the effect of the current sensor fault. In case of a single sensor fault, y_p^{i*} can be generated either according to physical redundancy of the three wire GSC interconnection (e.g., for a current sensor fault in phase a then $y_a^{i*}(k) = -y_b^i(k) - y_c^i(k)$), or according to the estimation of the fault as given by,

$$y_p^{i*}(k) = y_p^i(k) - \mathcal{D}_p [\hat{f}_p^i(k)], \quad (25)$$

where the dead-zone operator is illustrated in (24). In case of multiple current sensor faults, the physical redundancy cannot be used in the accommodation process and thus, the accommodation is achieved only by the estimation of the fault according to (25).

E. Design Guidelines for the FDIA scheme

The necessary steps through the design process of the proposed FDIA scheme are:

- 1) Adaptive state estimator design: As a first step for each phase, the adaptive state estimation scheme presented in (13)-(15) has to be designed. The design parameters λ_p^i , γ_p and ξ , are selected such that to succeed the necessary performance of the scheme, while they need to satisfy the following criteria: $|A - \lambda_p^i| \leq 1$, $\gamma_p > 0$, $-1 < \xi \leq 0$.
- 2) Residual generation: The current residual has to be implemented according to (16).
- 3) Adaptive threshold: The adaptive threshold of (21) needs to be constructed using the following stability criterion: $|A - \lambda_p^i| \leq \alpha_p \leq 1$.
- 4) Isolation Decision Logic: The isolation decision logic presented in Algorithm 1, needs to be implemented in order to exclude false alarms when grid faults occur.
- 5) Virtual current sensor: For accommodation purposes, the virtual current sensor signal of (25), needs to be developed, and provided to the GSC controller.

IV. SIMULATION AND EXPERIMENTAL RESULTS

A. Description of the system

In this section, simulation results are presented to show the effectiveness of the proposed FDIA methodology that is applied on a 1.8-kW three-phase GSC. For this purpose, a dynamic discrete model of an advanced GSC that can operate under any grid condition has been developed in MATLAB/Simulink according to the structure presented in Fig. 1. The GSC for interconnecting RES is actually a typical three-phase two-level PWM voltage source converter based on six switching Insulated-Gate Bipolar Transistors (IGBTs). The GSC injects high quality currents into the grid through an LC

TABLE I
DESIGN PARAMETERS OF THE SYSTEM

Module	Design Parameters
GSC nominal values	$P_{rated} = 1.8$ kW, $v_{LL-rated} = 230$ V, $f_{nominal} = 50$ Hz, $V_{dc} = 500$ V.
LC filter	$L_{cf} = 7.6$ mH, $R_{cf} = 0.19$ Ω $R_{f\Delta} = R_{fY}/3 = 1.1$ Ω , $C_{f\Delta} = C_{fY}/3 = 5.95$ μ F.
Sampling Frequency	$f_s = \frac{1}{T_s} = 3450$ Hz.
PWM frequency	$f_{PWM} = 3450$ Hz.
DN $\alpha\beta$ -PLL	$K_p = 92, T_I = 0.000235$ $\omega_f = 33.3\pi$ rad/s.
Current Controller	$K_p = 14.3, K_I = 218.5$ $K_{I-1} = 200, K_{I-5} = K_{I+5} = 100$, $K_{I-7} = K_{I+7} = 100$.
FDIA scheme	$\lambda_p^i = 0.05, \gamma_p = 0.58$ $\xi = -0.3, \bar{x}_p = 7$ A, $v_{sensor-rated} = 400$ V $\Delta A = 0.1A, \Delta B = 0.1B$ $\bar{n}_p^i = 0.008\bar{x}_p, \bar{h}_p = 0.05\bar{x}_p$ $\bar{n}_p^d = 0.01\sqrt{2}v_{sensor-rated}$

filter. The LC filter is designed according to the methodology proposed in [25] to eliminate high-order harmonics caused by the high switching frequency. The GSC controller is implemented in the synchronous reference frame (dq -frame) using Proportional-Integral (PI) controllers and includes a synchronization method, a current controller, and a PQ controller. The sampling frequency (f_s) and the switching PWM frequency (f_{PWM}) are both set to 3450 kHz. The synchronization of the GSC controller is achieved by an advanced phase-locked loop based algorithm, named DN $\alpha\beta$ -PLL as proposed in [3], that tracks accurately and fast the voltage phase angle under any grid conditions (i.e., harmonic distortion, grid fault). The current controller [3] ensures the high quality current injection under normal and abnormal (i.e., unbalanced low voltage grid faults) operation. An advanced PQ controller that enables the proper operation of the GSC even under grid faults has been designed according to [3], [23], [26]. The PQ controller can provide support to the grid under short circuit events in order to enhance the stability of the power system under high penetration of RES. Moreover, the PQ controller can regulate the active power (P) injection by maximizing the produced energy of RES, based on the DC-link voltage controller and the Maximum Power Point Tracking (MPPT) controller. The reactive power (Q) is regulated according to the Q -profile controller in order to improve the voltage stability of the grid. It should be noted that the accuracy of the developed GSC model has been validated according to experimental results in previous works [3], [23], [26] and thus, the simulation model can be trusted for validating the proposed FDIA scheme. All the design and tuning parameters of the dynamic GSC model are presented in Table I.

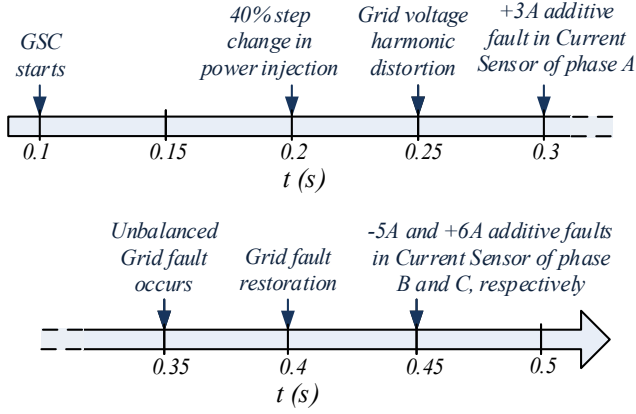


Fig. 3. Time schedule of the case study simulation scenario.

B. Simulation Results

This case study investigates the performance of the proposed FDIA scheme under several grid conditions and under different single sensor faults. The time schedule that has been followed in this simulation scenario is presented analytically in Fig. 3. Specifically, in order to examine the robustness of the proposed FDIA scheme, an abrupt 40% step change of the power injection is introduced at $t = 0.2$ s (i.e., the injected power changes from 40% to 80% of the rated power), followed by the injection of harmonic distortion on the grid voltage (e.g., 3% of fifth and 2% of seventh harmonics) at $t = 0.25$ s, and an unbalanced low-voltage grid fault (e.g., two phases to ground short circuit fault) at $t = 0.4$ s. Different additive abrupt (i.e., $\rho_p \rightarrow \infty$, $\forall p \in \mathcal{P}$) current sensor faults occur at $t = 0.3$ s and $t = 0.45$ s, with a single sensor fault with magnitude $f_a^i = 3$ A in phase a , and simultaneous current sensor faults $f_b^i = -5$ A in phase b , $f_c^i = 6$ A in phase c , respectively.

The detection and isolation process of the FDIA scheme is presented in Fig. 4, where the absolute value of the output residual $|\varepsilon_{y_p}^i|$, and the adaptive threshold $\bar{\varepsilon}_{y_p}^i$, $\forall p \in \mathcal{P} = \{a, b, c\}$ are presented. Moreover, Fig. 4 presents the isolation decision signal D_p (green dashed line) and the operation of the GFCU indicated by G_f (last graph). Fig. 5 presents the effectiveness of the proposed current sensor FDIA scheme, where the responses of the actual line currents x_p , $\forall p \in \mathcal{P} = \{a, b, c\}$ with FDIA scheme (blue solid line) and without the FDIA scheme (red dashed line) are illustrated.

Analytically, in Fig. 4(a), it can be seen that the sensor fault in phase a that occurs at $t = 0.3$ s, causes the violation of the adaptive threshold $\bar{\varepsilon}_{y_a}^i$ by the corresponding absolute value of the residual $|\varepsilon_{y_a}^i|$ and as a result the isolation decision logic D_a turns from 0 into 1, indicating that a sensor fault is detected and isolated in phase a . Accordingly, in phase b and phase c as it is shown in Fig. 4(b) and Fig. 4(c), at $t = 0.45$ s, the simultaneous current sensor faults $f_b^i = -5$ A and $f_c^i = 6$ are properly detected and isolated. It is worth mentioning that in Fig. 4(b) at $t = 0.35$ s two sensor faults are detected (i.e., false alarm) by the ARR \mathcal{E}_b and \mathcal{E}_c , but afterwards it are ignored (i.e., D_b, D_c set from 1 to 0) since the GFCU also detects a grid fault simultaneously (i.e., $G_f=1$) as it is shown

is Fig. 4(d). Generally, Fig. 4(a)-4(c) show that the detection is not affected either by the abrupt 40 % step change of the power injection at $t = 0.2$ s, or by the harmonic distortion affect the grid voltage at $t = 0.25$ s, since any of the \mathcal{E}_p , $\forall p \in \mathcal{P} = \{a, b, c\}$, are not violated. It is very important to indicate that the response of previous works in the literature about FDIA has only been tested under ideal grid conditions and thus, the FDIA effectiveness cannot be guaranteed under any grid operating conditions. A significant contribution of this paper is that the proposed FDIA scheme is tested under several normal and abnormal conditions and therefore, the response of the FDIA is tested under more realistic scenarios.

The beneficial effect of the proposed FDIA scheme on the GSC operation is demonstrated in Fig. 5 for the aforementioned sensor fault scenario. Particularly, in Fig. 5(a)-(c), the actual line currents x_a, x_b, x_c are presented for the case where the FDIA scheme is not used (red dashed lines), and for the case where the FDIA scheme is applied on the GSC controller (blue solid lines). In case where the FDIA scheme is not used, it is obvious that the actual line currents of the GSC violate the converter current limits (green dashed line). Such operation by the GSC can trip the protections of the GSC and cause the disconnection of the entire RES) or even worse can cause catastrophic failures to the GSC if the protections do not operate properly. On the contrary, if the proposed FDIA scheme is used, the method can in real-time detect and isolate the fault in each phase and further, a proper accommodation can be achieved since the sensor faults are fast and accurately estimated by the \hat{f}_p^i , $\forall p \in \mathcal{P} = \{a, b, c\}$ as shown in Fig. 5(d). As a result, the sensor faults are properly accommodated and the GSC can achieve an appropriate operation as shown by the actual currents (blue solid lines) in Fig. 5(a)-(c).

An extensive investigation of the effectiveness of the proposed FDIA scheme has been performed under several scenarios. The FDIA scheme has been tested under a variation of the LC filter parameters within a range of $\pm 10\%$, under grid frequency faults, under several grid voltage faults and under several harmonic distortion conditions. In all cases, the FDIA scheme achieves a proper operation without causing false alarms. Further, the FDIA scheme has been tested under several operating conditions of the GSC, and under several sensor faults. It is worth mentioning that the proposed scheme can properly operate when the GSC is injecting 5%-100% of its rated power and when a current sensor fault occurs with an additive offset of 5%-100% of the nominal current.

C. Experimental verification

In this section, the proposed FDIA scheme is verified experimentally. In Fig. 6, a photo of the experimental setup used to obtain the results showed in Fig. 7 is presented. The following experimental setup of Fig. 6 is configured according to: (i) a grid tied inverter (SEMIKRON Semiteach B6U+E1C1F+B6CI), (ii) a DC power supply (EA-PS 9750-20) for emulating the injected power by a renewable into the DC-link, and (iii) a dSPACE (DS 1104) controller board where the GSC controller and the proposed FDIA scheme have been developed by using the MATLAB/Simulink Real Time Interface. The sensors used for this setup are: (i) three

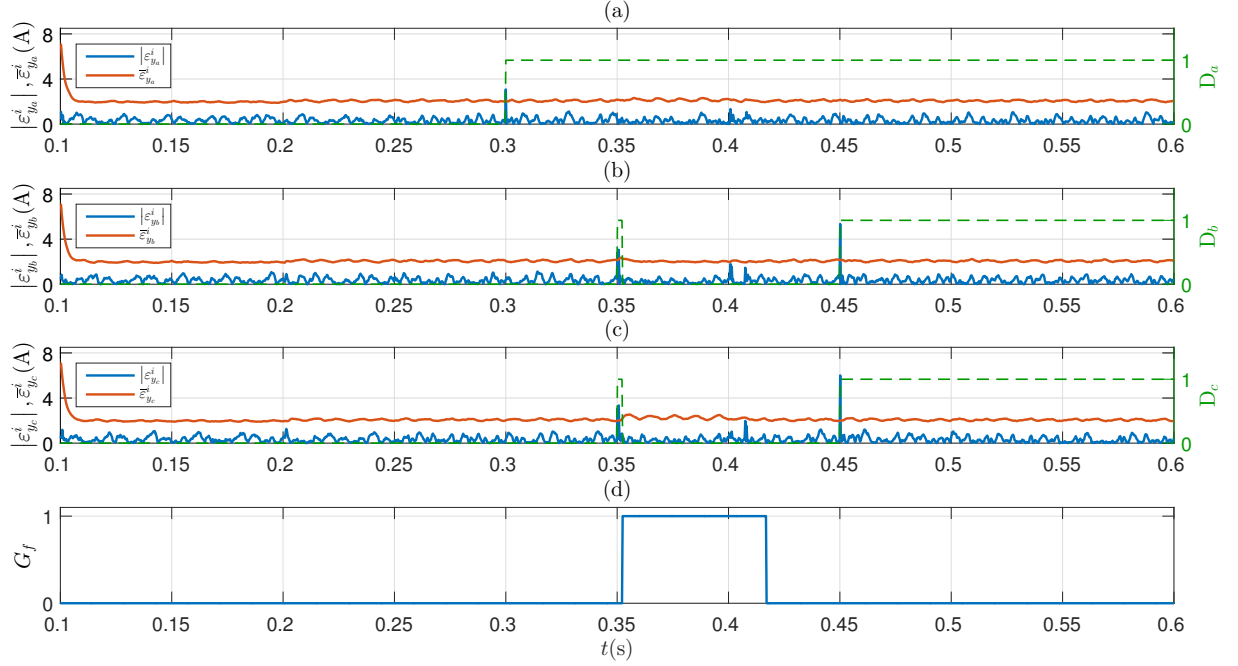


Fig. 4. The detection and isolation process of the first case study (see Section IV-B). In (a)-(c), the absolute value of the residual $|e_{y_p}^i|$ (blue solid line) and the adaptive threshold $\bar{e}_{y_p}^i$ (red solid line) for each phase, $p \in \mathcal{P} = \{a, b, c\}$ are presented. The green dashed line (right vertical axis) indicates the isolation decision signal D_p . In (d) the boolean decision signal G_f is presented, which shows the operation of the GFCU.

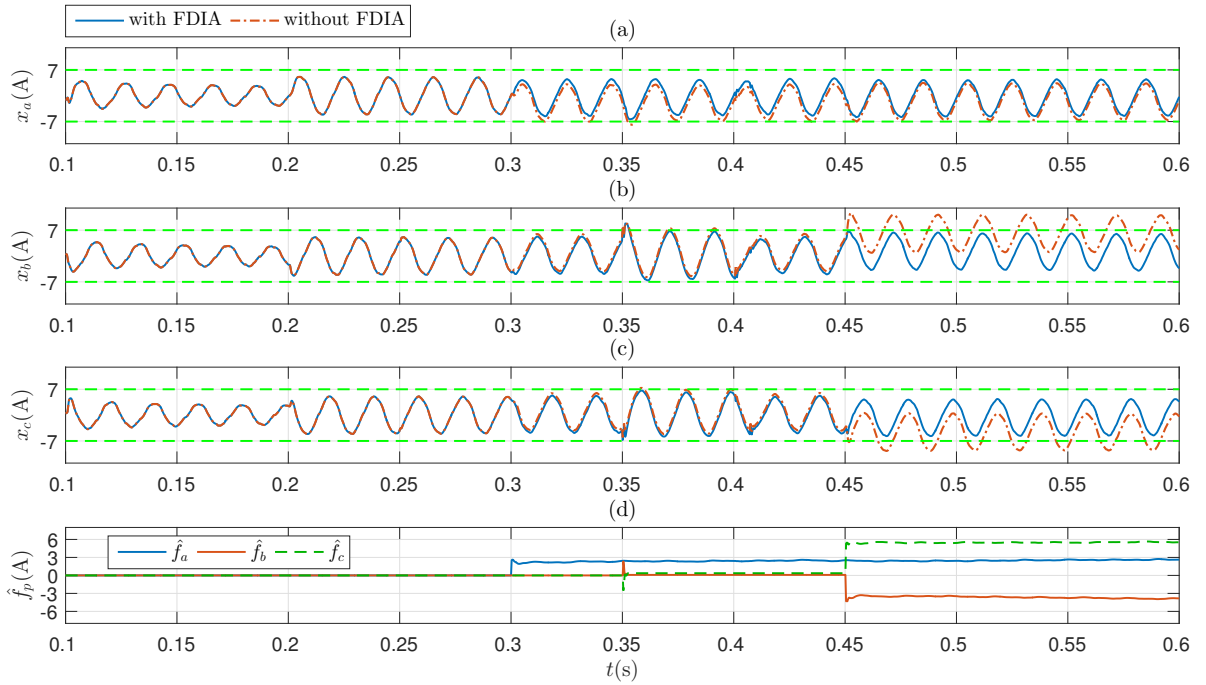


Fig. 5. The effectiveness of the current sensor FDIA scheme in the first case study (see Section IV-B). In (a)-(c), the actual line current x_p , for each phase $p \in \mathcal{P} = \{a, b, c\}$, of the GSC without the FDIA scheme (red dashed line) and with the FDIA scheme (blue solid line) are presented. The green dashed line in (a)-(c), indicates the protection current limits of the GSC. In (d) the estimation of the sensor fault magnitudes \hat{f}_p^i , $\forall p \in \mathcal{P} = \{a, b, c\}$ are presented.

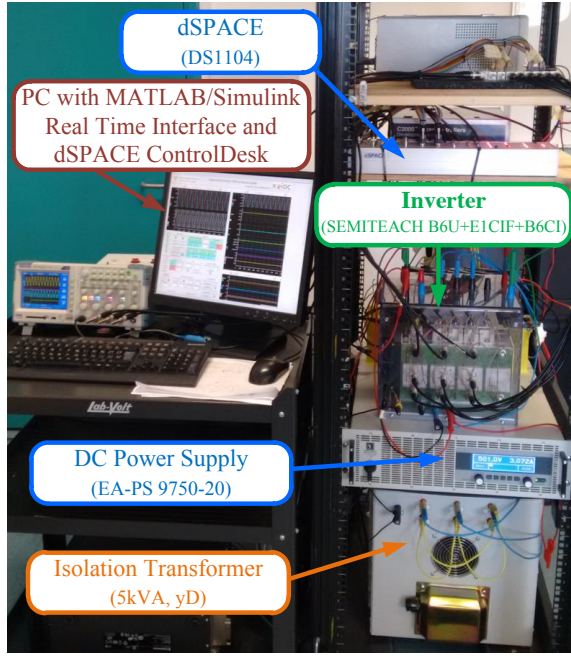


Fig. 6. The experimental setup. The proposed sensor FDIA scheme is executed in real-time on the dSPACE controller board.

current sensors (i.e., LEM LTSR 6-NP), with upper noise bound $n_p^i = 0.008\bar{x}_p$ and (ii) three voltage sensors (i.e., LEM LV25-400) with upper noise bound $n_p^d = 0.01\sqrt{2}v_{sensor-rated}$. Fig. 7 shows the effectiveness of the proposed FDIA scheme, under the occurrence of a single sensor fault in phase-a with $f_a^i = 3$ A. Analytically, in Fig. 7 the experimental results for phase a , without and with the current sensor fault FDIA scheme are presented. In Fig. 7(a) the actual line current x_a of the GSC is presented, without accommodation (orange solid line), and in Fig. 7(b) the actual line current x_a is presented, with accommodation (orange solid line). The blue dashed line indicates the fault-free current limits of the GSC. In both graphs (Fig. 7(a) and Fig. 7(b)), the residual $\varepsilon_{y_a}^i$ (cyan solid line) and the adaptive threshold (purple solid line) are presented. Specifically, in Fig. 7(a), can be observed that the actual line current of GSC in phase a (x_a), violates fault-free current limits of the GSC, which means that in Fig. 7(a), where the FDIA scheme is implemented, the actual current remains very close to the fault-free (pre-fault) operation. Note that the sensor fault magnitude in the experimental results is selected to be small in order to avoid reaching over-current protection limits, which will enforce the system to trip. However, besides the selection of a small sensor fault magnitude, the proposed current sensor FDIA scheme detects, isolates and accommodates it.

Further, it is important to note that the computational burden of the method has also been investigated using Simulink's profile report and it is shown that the extra required processing time for executing the proposed method is not prohibitive (increased by 15.2%) for the development of the method in real-time power electronic applications.

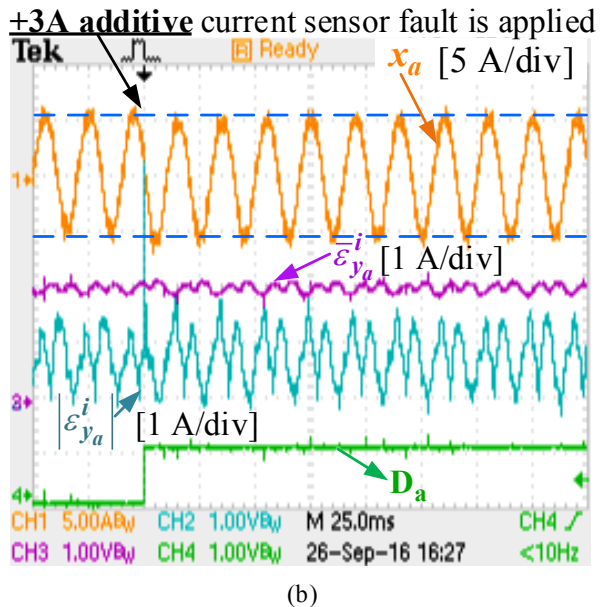
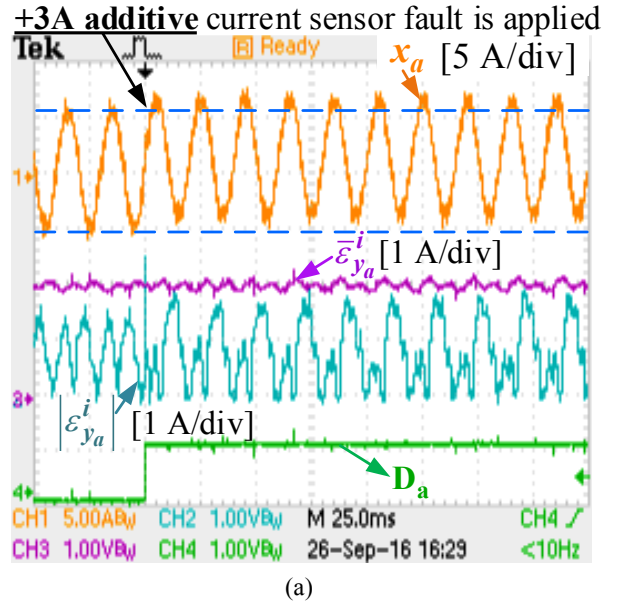


Fig. 7. The effectiveness of the current sensor FDIA scheme in the experimental study (see Section IV-C). In (a) the actual line current x_a of the GSC without accommodation (orange solid line), and in (b) with accommodation (orange solid line) are presented. The blue dashed line indicates the over-current protection limits of the GSC. In both graphs ((a) and (b)), the residual $\varepsilon_{y_a}^i$ (cyan solid line) and the adaptive threshold (purple solid line) are presented.

V. CONCLUSION

This work proposes a robust current sensor FDIA scheme for the GSC of RES. The method relies on analytical redundancy relations (i.e., the generation of residuals and adaptive thresholds for each phase of the grid side converter). An isolation decision logic has been developed which takes into consideration of the analytical redundancy relations and the operating condition of a fault classification unit in order to distinguish between current sensor faults and grid faults. Once a current sensor fault is isolated, an accommodation

scheme compensate the effects of the current sensor fault. As a result, the GSC can keep its proper operation without risking the reliability of the converter and without causing the disconnection of the entire RES. Further, an investigation of the effectiveness of the proposed scheme has been performed for all possible operating conditions of the GSC and under any possible grid condition. Beside the simulations results that validate the performance of the proposed methodology, it has been also tested in a real experimental setup.

APPENDIX A

STABILITY ANALYSIS OF ADAPTIVE ESTIMATION SCHEME

The stability analysis of the proposed adaptive estimation scheme developed in (13)-(15) under faulty conditions (i.e., $f_p^i \neq 0$) is provided below.

Theorem 1: Under the Assumptions 1-2, the stability property of the adaptive estimation scheme shown in (13)-(15) is guaranteed, if $\varepsilon_{x_p}^i \in L_\infty$ and $\hat{f}_p^i \in L_\infty$ implies that $\lim_{k \rightarrow \infty} \varepsilon_{x_p}^i(k) = 0$ and $\lim_{k \rightarrow \infty} \tilde{f}_p^i(k) = 0$, where $\varepsilon_{x_p}^i$ is the state estimation error obtained in (13) and \tilde{f}_p^i is the sensor fault estimation error, which is defined as $\tilde{f}_p^i = f_p^i - \hat{f}_p^i$.

Proof: Under a single sensor fault and without considering modeling uncertainties (i.e., $\Delta A = 0$, $\Delta B = 0$, $h_p(x_p) = 0$) and sensor noise, the dynamics of $\varepsilon_{x_p}^i$ are given by,

$$\varepsilon_{x_p}^i(k+1) = x_p(k+1) - \hat{x}_p(k+1) \quad (26)$$

$$= (A - \lambda_p^i) \varepsilon_{x_p}^i(k) - \lambda_p^i \tilde{f}_p^i(k) - \Omega_p(k) (\hat{f}_p^i(k+1) - \hat{f}_p^i(k)). \quad (27)$$

Subtracting $\Omega_p(k)$ in both sides of (14) and rearranging it, $-\lambda_p^i$ can be expressed as,

$$-\lambda_p^i = \Omega_p(k+1) - \Omega_p(k) - (A - \lambda_p^i - 1) \Omega_p(k). \quad (28)$$

Since, $f_p^i(k+1) = f_p^i(k)$ (i.e., constant fault magnitude at the steady state) we can conclude that,

$$\hat{f}_p^i(k+1) - \hat{f}_p^i(k) = -(\tilde{f}_p^i(k+1) - \tilde{f}_p^i(k)).$$

By replacing $-\lambda_p^i$ on (27), the dynamics of the state estimation error are given as,

$$\begin{aligned} \varepsilon_{x_p}^i(k+1) - \varepsilon_{x_p}^i(k) &= (A - \lambda_p^i - 1) (\varepsilon_{x_p}^i(k) - \Omega_p(k) \tilde{f}_p^i(k)) \\ &\quad + (\Omega_p(k+1) - \Omega_p(k)) \tilde{f}_p^i(k) \\ &\quad - \Omega_p(k) (\hat{f}_p^i(k+1) - \hat{f}_p^i(k)). \end{aligned} \quad (29)$$

By letting $\varepsilon_{z_p}^i(k) = \varepsilon_{x_p}^i(k) - \Omega_p(k) \tilde{f}_p^i(k)$, (29) can be expressed as,

$$\varepsilon_{z_p}^i(k+1) = (A - \lambda_p^i) \varepsilon_{z_p}^i(k), \quad (30)$$

where λ_p^i is chosen to satisfy $(A - \lambda_p^i) \leq 1$ such that $\lim_{k \rightarrow \infty} \varepsilon_{z_p}^i(k) = 0$, and as a result $\lim_{k \rightarrow \infty} \varepsilon_{x_p}^i(k) = 0$ and $\lim_{k \rightarrow \infty} \tilde{f}_p^i(k) = 0$.

REFERENCES

[1] F. Blaabjerg and K. Ma, "Future on power electronics for wind turbine systems," *IEEE Journal of Emerging and Selected Topics in Power Electronics*, vol. 1, no. 3, pp. 139–152, Sep. 2013.

[2] A. Izadian, N. Girrens, and P. Khayyer, "Renewable Energy Policies: A Brief Review of the Latest U.S. and E.U. Policies," *IEEE Mag. Industrial Electronics*, vol. 7, no. 3, pp. 21–34, Sep. 2013.

[3] L. Hadjidemetriou, E. Kyriakides, and F. Blaabjerg, "A Robust Synchronization to Enhance the Power Quality of Renewable Energy Systems," *IEEE Trans. Industrial Electronics*, vol. 62, no. 8, pp. 4858–4868, Aug. 2015.

[4] B. Craciun, T. Kerekes, D. Sera, and R. Teodorescu, "Overview of recent grid codes for PV power integration," in *Proc. OPTIM*, Brasov, 2012, pp. 959–965.

[5] L. Hadjidemetriou, E. Kyriakides, Y. Yang, and F. Blaabjerg, "A Synchronization Method for Single-Phase Grid-Tied Inverters," *IEEE Trans. Power Electronics*, vol. 31, no. 3, pp. 2139–2149, Mar. 2016.

[6] L. Hadjidemetriou, P. Demetriou, and E. Kyriakides, "Investigation of different fault ride through strategies for renewable energy sources," in *Proc. IEEE POWERTECH*, 2015, pp. 1–6.

[7] J. Rocabert, A. Luna, F. Blaabjerg, and P. Rodriguez, "Control of power converters in AC microgrids," *IEEE Trans. Power Electronics*, vol. 27, no. 11, pp. 4734–4749, Nov. 2012.

[8] I. Jlassi, J. O. Estima, S. Khojot El Khil, N. Mrabet Bellaaj, and A. J. Marques Cardoso, "Multiple open-circuit faults diagnosis in back-to-back converters of PMSG drives for wind turbine systems," *IEEE Trans. Power Electronics*, vol. 30, no. 5, pp. 2689–2702, 2015.

[9] Z. Wang, Z. Huang, C. Song, and H. Zhang, "Multiscale adaptive fault diagnosis based on signal symmetry reconstitution preprocessing for microgrid inverter switch under changing load condition," *IEEE Trans. Smart Grid*, pp. 1–10, 2016 (Early access article).

[10] T. Kamel, Y. Biletskiy, C. P. Diduh, and L. Chang, "Fault diagnoses for all the stages of the power electronic converter," in *Proc. IEEE CCECE*, April 2012, pp. 1–4.

[11] —, "Open circuit fault diagnoses for power electronic converters," in *Proc. IEEE ISIE*, June 2015, pp. 361–366.

[12] T. Kamel, Y. Biletskiy, and L. Chang, "Real-time diagnosis for open-circuited and unbalance faults in electronic converters connected to residential wind systems," *IEEE Trans. Industrial Electronics*, vol. 63, no. 3, pp. 1781–1792, 2016.

[13] H. Berriri, M. W. Naouar, and I. Slama-Belkhdja, "Easy and fast sensor fault detection and isolation algorithm for electrical drives," *IEEE Trans. Power Electronics*, vol. 27, no. 2, pp. 490–499, 2012.

[14] K. Rothenhagen and F. W. Fuchs, "Current sensor fault detection by bilinear observer for a doubly fed induction generator," in *Proc. IEEE IECON*, 2006, pp. 1369–1374.

[15] P. Jain, J. X. Xu, S. K. Panda, J. Poon, C. Spanos, and S. R. Sanders, "Fault diagnosis via PV panel-integrated power electronics," in *Proc. IEEE COMPEL*, June 2016, pp. 1–6.

[16] S. Karimi, A. Gaillard, P. Poure, and S. Saadate, "Current sensor fault-tolerant control for WECS with DFIG," *IEEE Trans. Industrial Electronics*, vol. 56, no. 11, pp. 4660–4670, 2009.

[17] J. Chen and R. J. Patton, *Robust model-based fault diagnosis for dynamic systems*. Springer Science & Business Media, 2012, vol. 3.

[18] M. Blanke, M. Kinnaert, J. Lunze, M. Staroswiecki, and J. Schröder, *Diagnosis and fault-tolerant control*. Springer, 2006, vol. 2.

[19] V. Reppa, M. M. Polycarpou, and C. G. Panayiotou, "Decentralized isolation of multiple sensor faults in large-scale interconnected nonlinear systems," *IEEE Trans. Automatic Control*, vol. 60, no. 6, pp. 1582–1596, 2015.

[20] P. J. Antsaklis and A. N. Michel, *Linear systems*. Springer Science & Business Media, 2006.

[21] A. T. Vemuri and M. M. Polycarpou, "Robust nonlinear fault diagnosis in input-output systems," *International Journal of Control*, vol. 68, no. 2, pp. 343–360, 1997.

[22] J. A. Farrell and M. M. Polycarpou, *Adaptive approximation based control: Unifying neural, fuzzy and traditional adaptive approximation approaches*. Wiley-Interscience, 2006, vol. 48.

[23] L. Hadjidemetriou, E. Kyriakides, and F. Blaabjerg, "An Adaptive Tuning Mechanism for Phase-Locked Loop Algorithms for Faster Time Performance of Interconnected Renewable Energy Sources," *IEEE Trans. Industry Applications*, vol. 51, no. 2, pp. 1792–1804, Apr. 2015.

[24] M. Bollen, *Understanding power quality problems: Voltage sags and interruptions*. IEEE press, New York: Wiley, 2000, vol. 3.

[25] A. Reznik, M. G. Simoes, A. Al-Durra, and S. M. Mueyen, "LCL filter design and performance analysis for grid-interconnected systems," *IEEE Trans. Industry Applications*, vol. 50, no. 2, pp. 1225–1232, Apr. 2014.

[26] L. Hadjidemetriou, E. Kyriakides, and F. Blaabjerg, "A New Hybrid PLL for Interconnecting Renewable Energy Systems to the Grid," *IEEE Trans. Industry Applications*, vol. 49, no. 6, pp. 2709–2719, 2013.



Panayiotis M. Padopoulos (S'13) received the B.Sc. and M.Sc. degrees from the University of Cyprus, Nicosia, Cyprus, in 2012 and 2014, respectively, where he is currently pursuing the Ph.D. degree from the University of Cyprus, all in electrical engineering. His current research interests include fault diagnosis for distributed systems, nonlinear control theory, intelligent systems, and adaptive fault-tolerant control in HVAC Systems.

He is currently the Chair of IEEE University of Cyprus Student Branch from Feb. 2015.



Lenos Hadjidemetriou (S'11–M'16) received the Diploma in Electrical and Computer Engineering in 2010 from the National Technical University of Athens, Athens, Greece, and his Ph.D. degree in Electrical Engineering in 2016 from University of Cyprus. Currently, he is a Postdoctoral Research Fellow at the KIOS Research Center for Intelligent Systems and Networks, University of Cyprus. His research interests include renewable energy systems, grid synchronization methods, fault ride through control, power electronics, and micro-grids.

Dr. Hadjidemetriou is a member of the Cyprus Technical Chamber. He volunteered as a reviewer to several IEEE transactions and conferences and received the best paper award in the power quality session at IEEE IECON13.



Elias Kyriakides (S'00–M'04–SM'09) received the B.Sc. degree in Electrical Engineering from the Illinois Institute of Technology, Chicago, IL, USA, in 2000 and the M.Sc. and Ph.D. degrees in Electrical Engineering from Arizona State University, Tempe, AZ, USA, in 2001 and 2003, respectively.

He is currently an Associate Professor with the Department of Electrical and Computer Engineering, University of Cyprus, Nicosia. He is also a Founding Member of the KIOS Research Center for Intelligent Systems and Networks. His research interests

include modeling of electric machines, synchronized measurements in power systems, security and reliability of the power system networks, optimization of power system operation techniques, and the integration of renewable energy sources.



Marios M. Polycarpou (F'06) is a Professor of Electrical and Computer Engineering and the Director of the KIOS Research Center for Intelligent Systems and Networks at the University of Cyprus. His teaching and research interests are in intelligent systems and networks, adaptive and cooperative control systems, computational intelligence, fault diagnosis and distributed agents. He has published more than 300 articles in refereed journals, edited books and refereed conference proceedings, and co-authored 7 books. He is also the holder of 6 patents. Prof.

Polycarpou is a Fellow of the IEEE and IFAC, and has served as the President of the *IEEE Computational Intelligence Society* between Jan. 2012–Dec. 2013. He has served as the Editor-in-Chief of the *IEEE Transactions on Neural Networks and Learning Systems* between 2004–2010. He is the recipient of the 2016 IEEE Neural Networks Pioneer Award. Prof. Polycarpou has participated in more than 60 research projects/grants, funded by several agencies and industry in Europe and the United States, including the prestigious European Research Council (ERC) Advanced Grant.